Supplementary Information

Synergistic LSPR and interfacial built-in electric field in Au/WO_3 film for High-performance Flexible Electrochromic Smart Window

Yue Shen,[ab] Ying Lv,*[a] Pan Li,*[c] Shengze Li,[ab] Wentian Zhang,[ab] Xin You,[ab] Hangyu Ma,[ab] Guojiao Chen,[ab] Tienan Wang,[a] Xiaoyang Guo,[a] Xingyuan Liu*[a]

[a] *State key laboratory of luminescence science and technology, Changchun Institute of Optics, Fine Mechanics and Physics, Chinese Academy of Sciences, Changchun 130033, China.*

E-mail: lvying@ciomp.ac.cn; liuxy@ciomp.ac.cn

[b] *University of Chinese Academy of Sciences, Beijing 100049, China*

[c] *The Institute of Advanced Displays and Imaging, Henan Academy of Sciences, Zhengzhou, 450047, China.*
E-mail: lipan@hnas.ac.cn

This file includes:

Supplementary Figures S1-S24

Supplementary Tables S1

Supplementary References

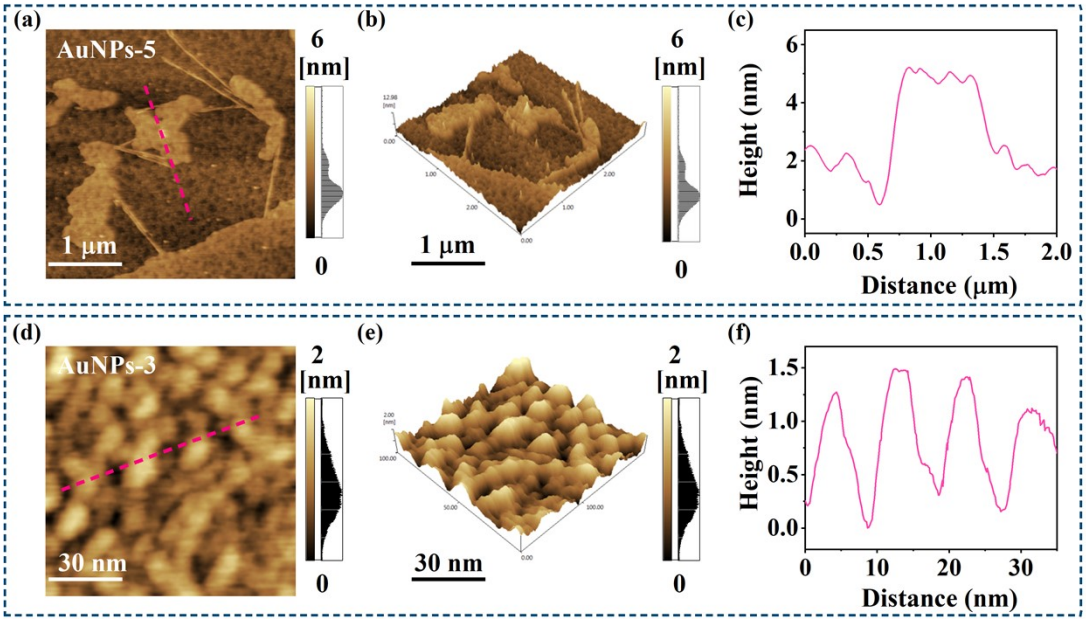

Fig. S1 (a,d) AFM images , (b,e) 3D AFM images and (c,f) corresponding height line-scan profiles of AuNPs-5 and AuNPs-3.

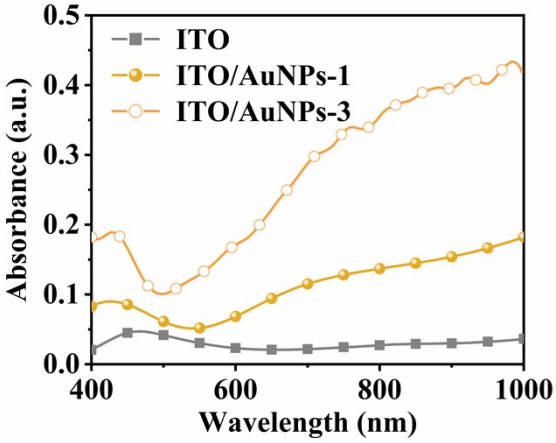

Fig. S2 Absorbance curve of Bare ITO, ITO/AuNPs-1 and ITO/AuNPs-3.

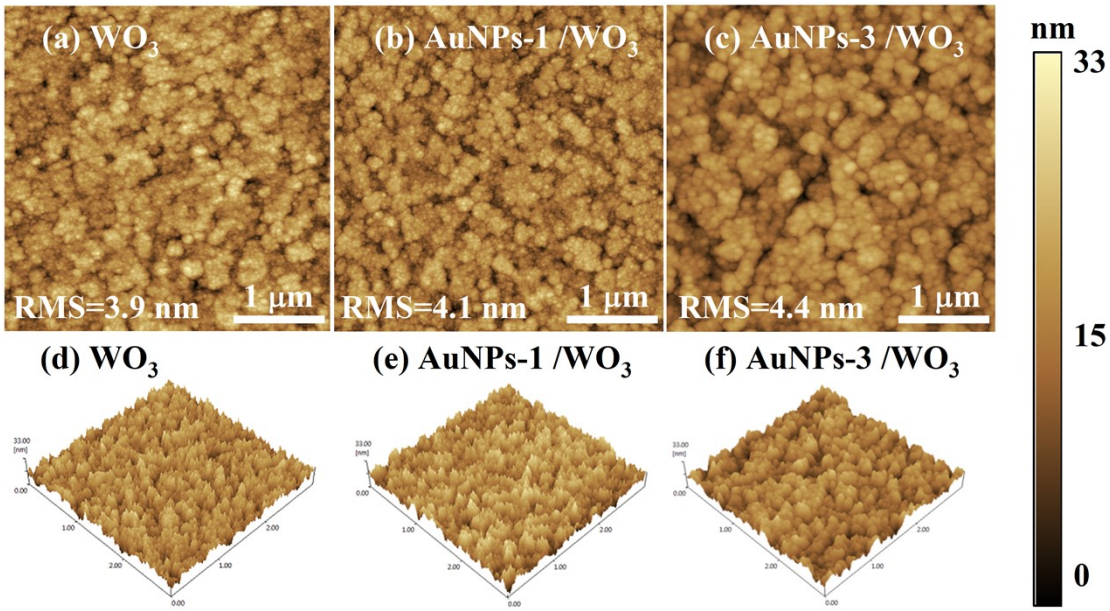

Fig. S3 The surface and 3D AFM images of (a, d) pure WO_3, (b, e) AuNPs-1 /WO_3, (c, f) AuNPs-3 /WO_3 films, respectively.

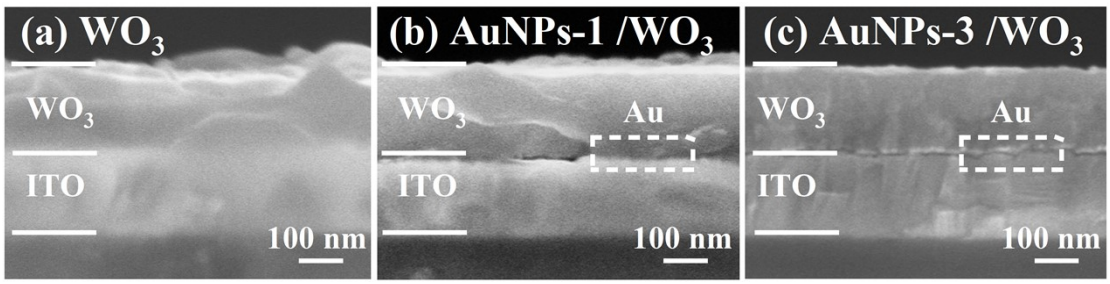

Fig. S4 Cross-section SEM images of (a) pure WO_3, (b) AuNPs-1 /WO_3, (c) AuNPs-3 /WO_3 films.

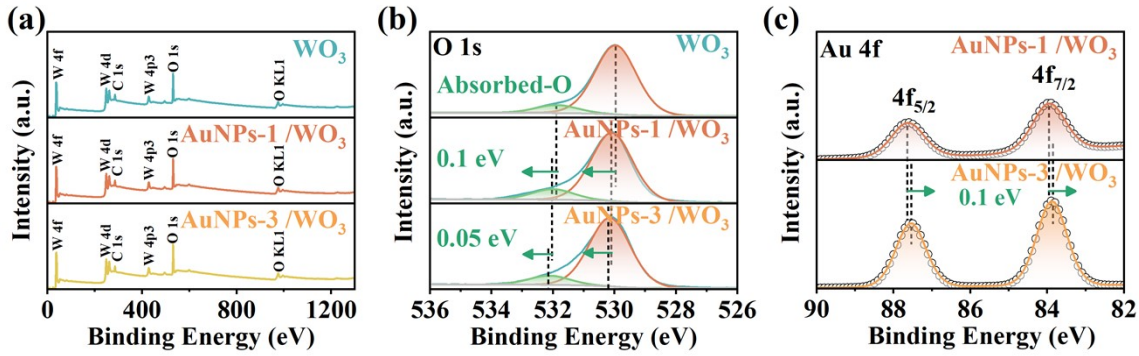

Fig. S5 (a) Full XPS profiles of pure WO_3, AuNPs-1 /WO_3, and AuNPs-3 /WO_3 with the WO_3 thickness of 150 nm. High-resolution XPS spectra of (b) O 1s in pure WO_3, AuNPs-1 /WO_3, and AuNPs-3 /WO_3 films with the WO_3 thickness of 10 nm and (c) Au 4f in AuNPs-1 /WO_3 and AuNPs-3 /WO_3 films.

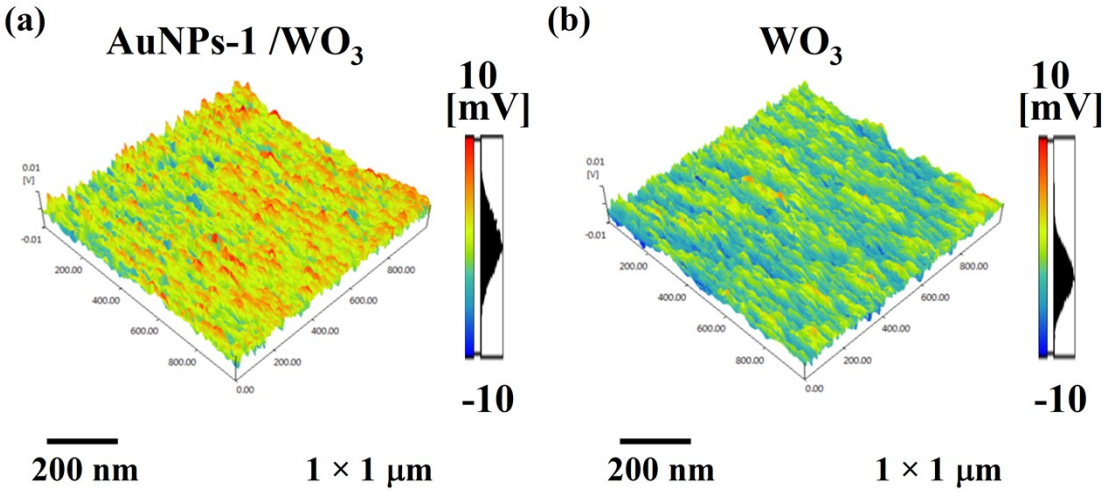

Fig. S6 3D KPFM images of (a) AuNPs-1 /WO_3 and (b) pure WO_3.

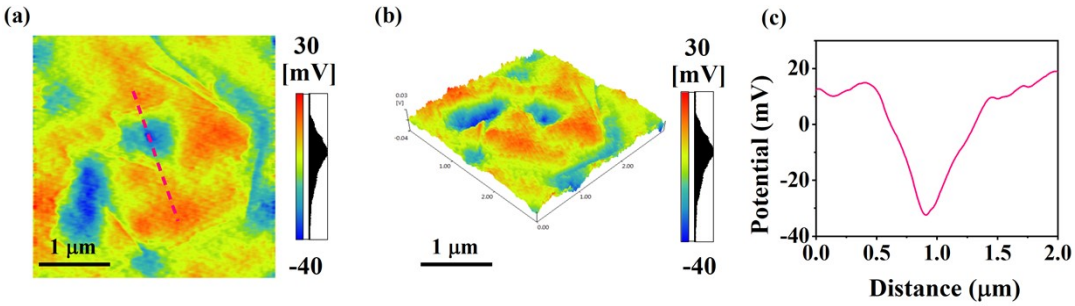

Fig. S7 (a) AFM images, (b) 3D AFM images and (c) corresponding height line-scan profiles, (d) KPFM images, (e) 3D KPFM images and (f) corresponding surface potential line-scan profiles of quasi-2D Au clusters/WO_3 film.

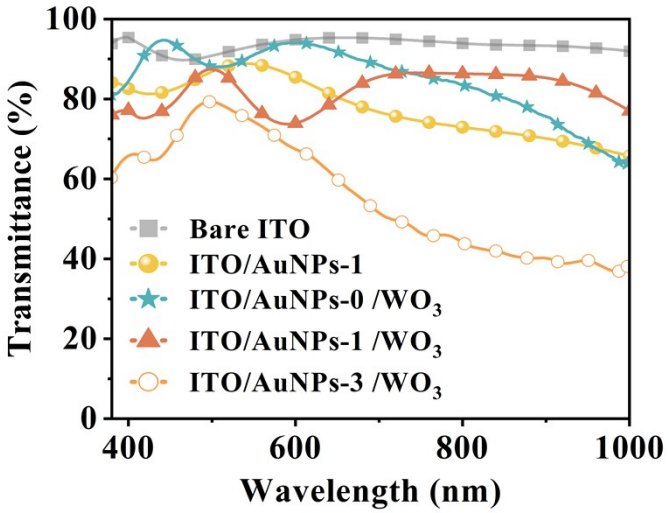

Fig. S8 The transmittance spectra of bare ITO, ITO/AuNPs-1, ITO/AuNPs-0 /WO_3, ITO/AuNPs-1 /WO_3 and ITO/AuNPs-3 /WO_3 films with air as the background.

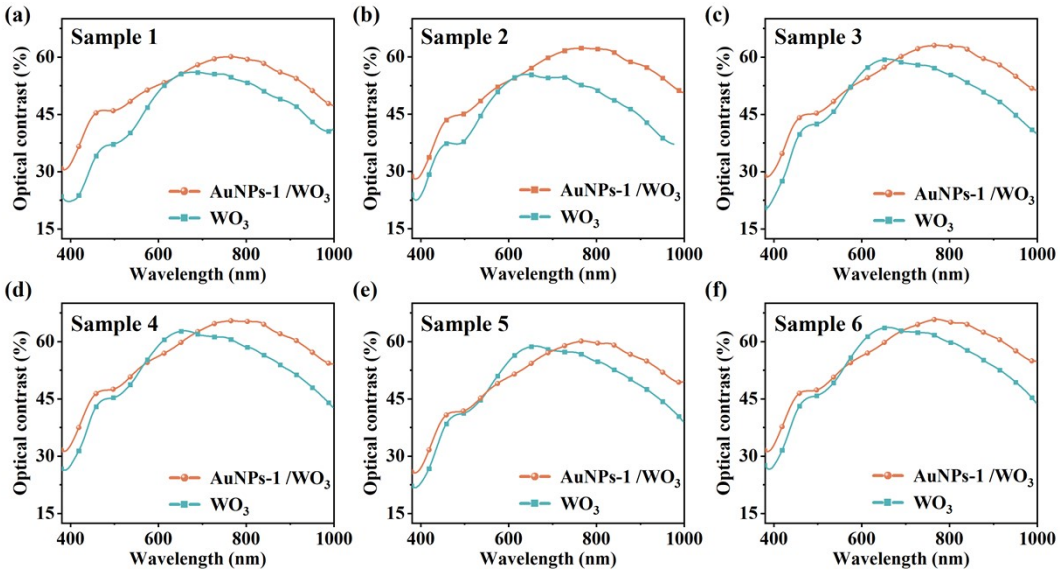

Fig. S9 Optical contrast at various wavelength of six AuNPs-1 /WO_3 films and pure WO_3 films.

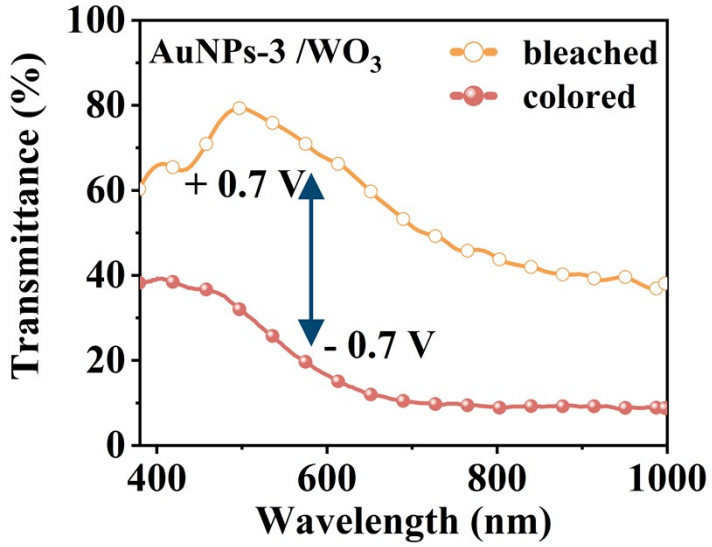

Fig. S10 Transmittance spectra of AuNPs-3 /WO_3 in the colored and bleached states under the potential of ± 0.7 V (vs. Ag/AgCl).

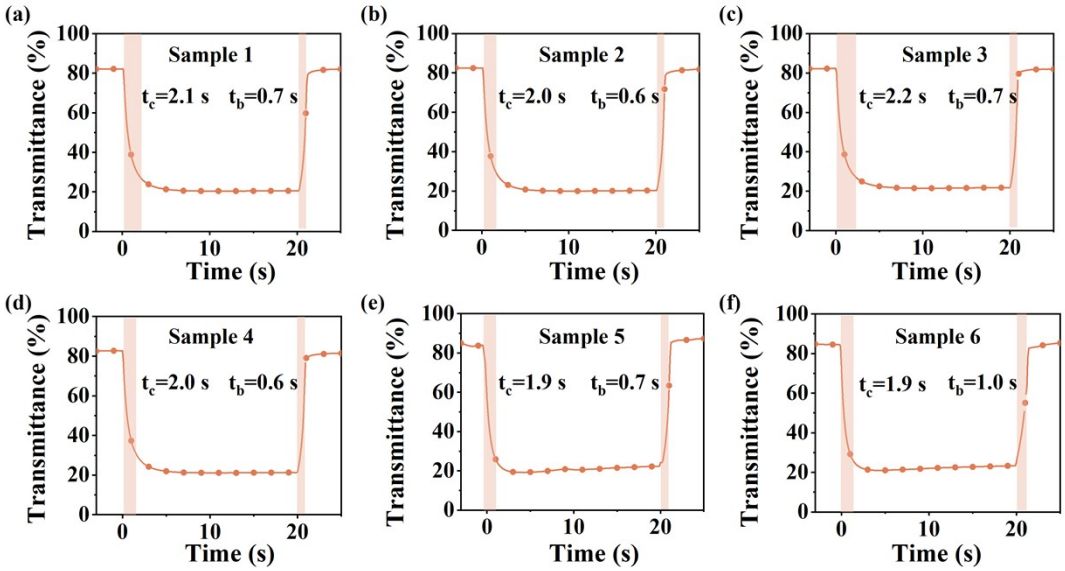

Fig. S11 In situ transmittance vs. time curves at 700 nm of six AuNPs-1 /WO_3 films.

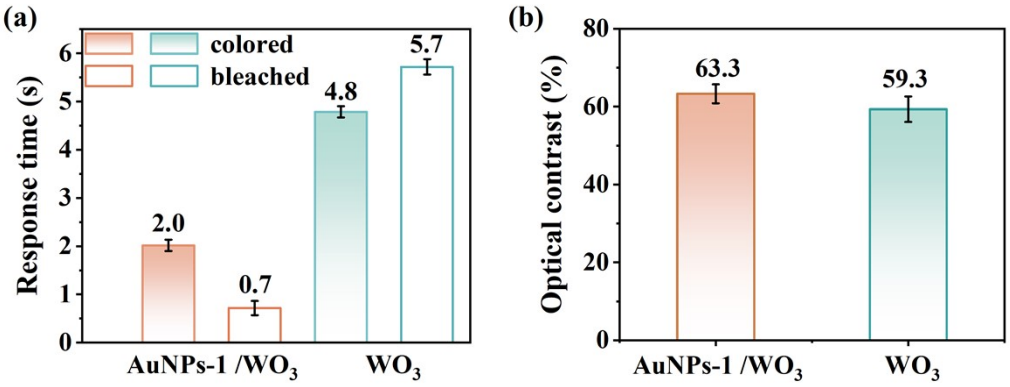

Fig. S12 Statistical diagram of response time and optical contrast of AuNPs-1 /WO_3 and pure WO_3 films.

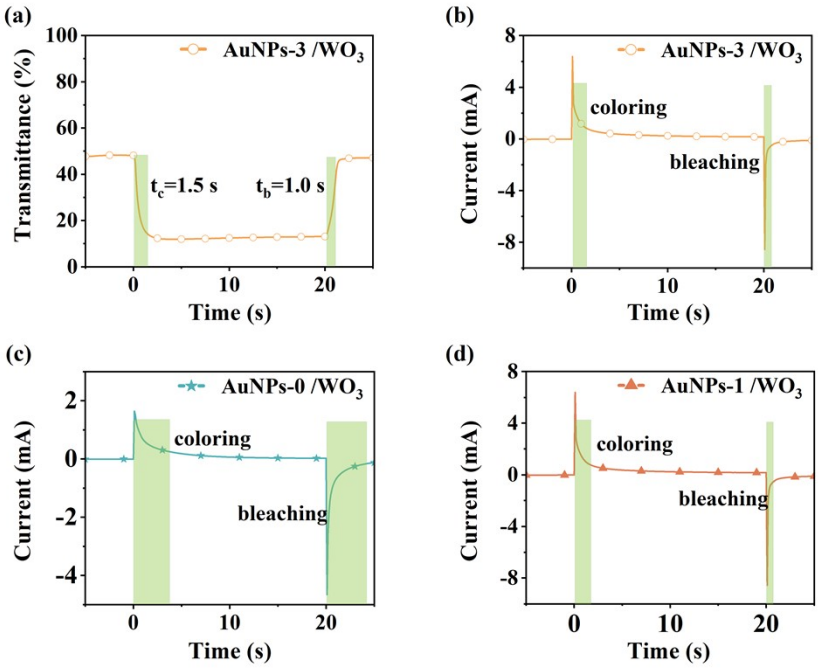

Fig. S13 (a) Transmittance vs. time curves of AuNPs-3 /WO_3 and current vs. time curves of (b) AuNPs-3 /WO_3, (c) WO_3, and (d) AuNPs-1 /WO_3 under potential of ±0.7 V (vs. Ag/AgCl) with 20 s intervals.

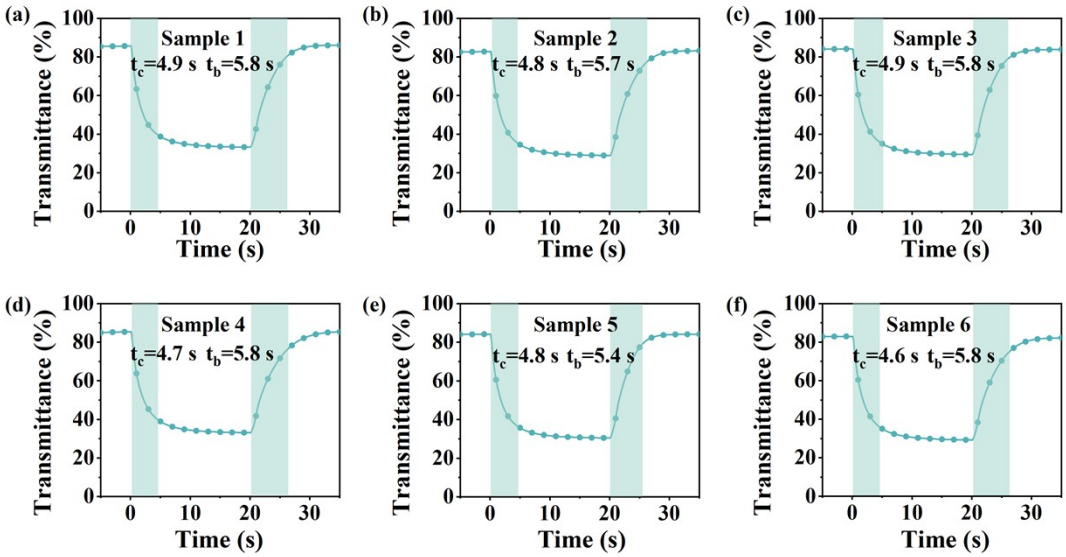

Fig. S14 In situ transmittance vs. time curves at 700 nm of six pure WO_3 films.

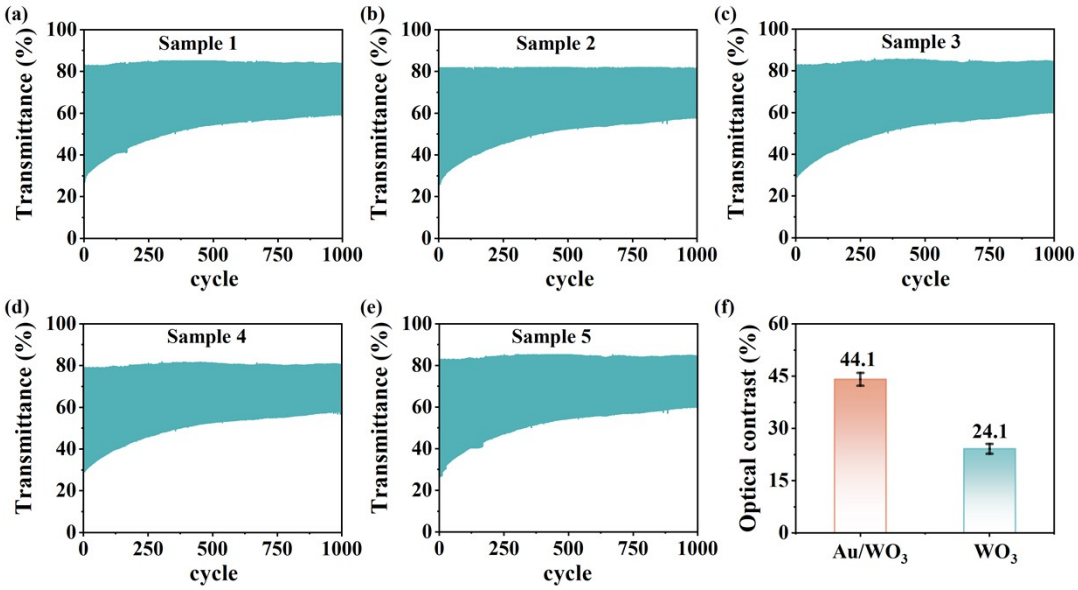

Fig. S15 In situ transmittance curves for 1000 EC cycles of 5 pure WO_3 films.

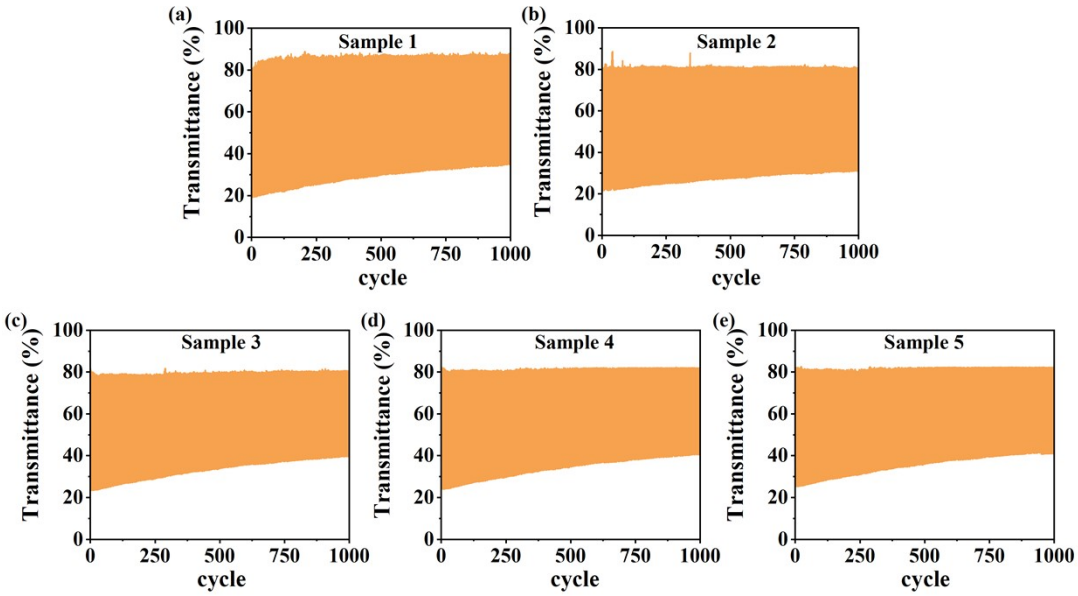

Fig. S16 In situ transmittance curves for 1000 EC cycles of 5 AuNPs-1 /WO_3 films.

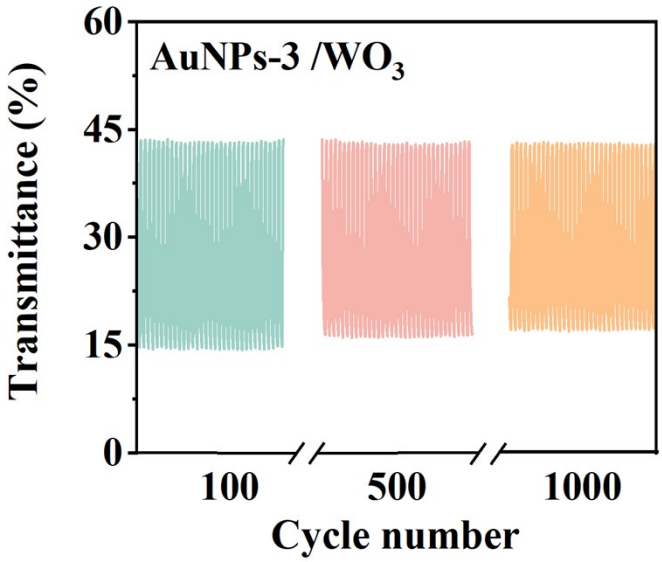

Fig. S17 *In situ* transmittance curves of AuNPs-3 /WO_3 film for 1000 EC cycles .

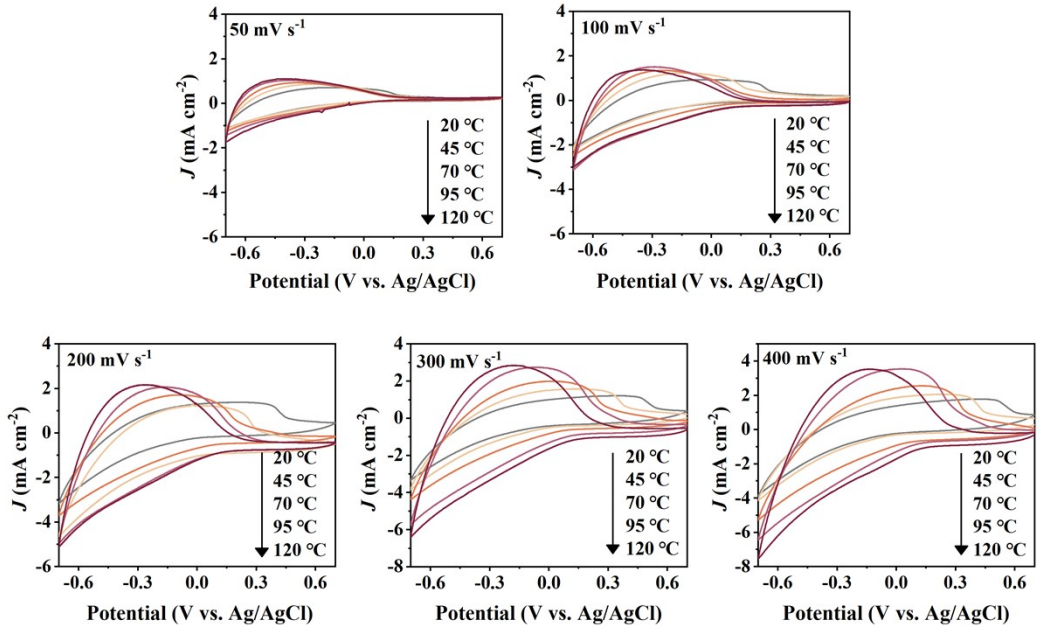

Fig. S18 CV curves of AuNPs-1 /WO_3 film at different temperatures.

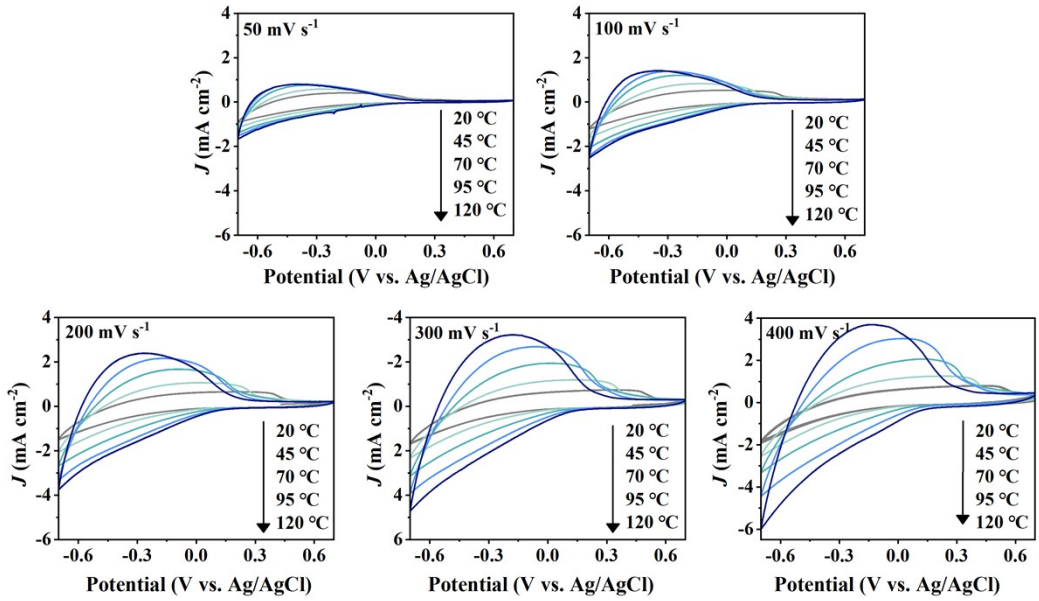

Fig. S19 CV curves of pure WO_3 film at different temperatures.

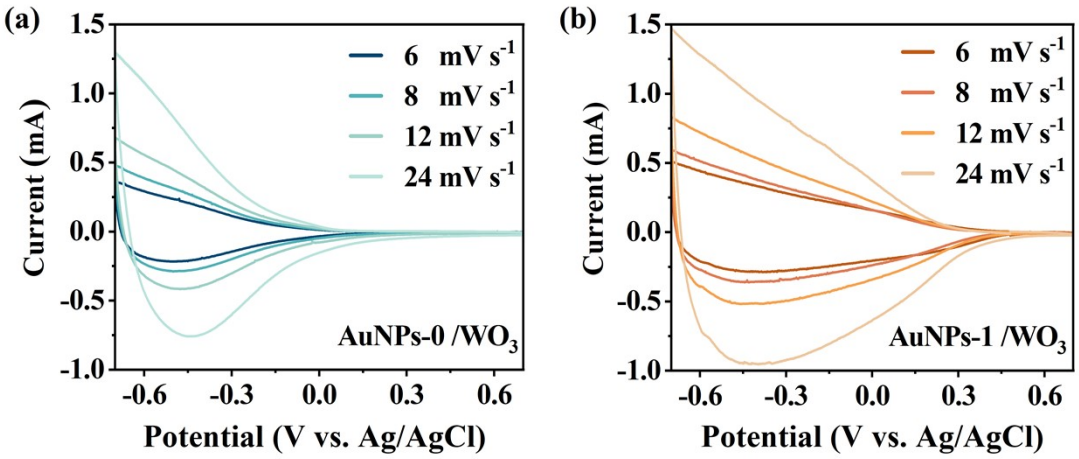

Fig. S20 CV curves for (a) AuNPs-1 /WO_3 and (b) WO_3 at the scan rate of 6, 8, 12, 24 mV s^{-1}, respectively.

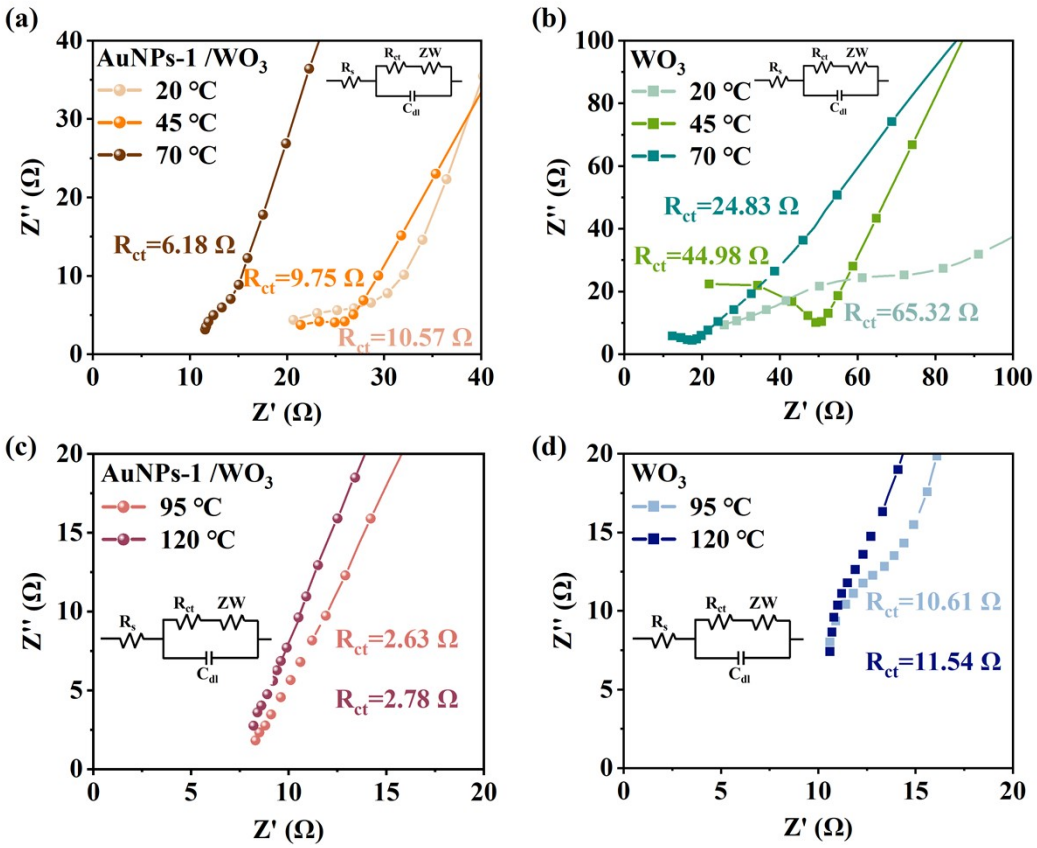

Fig. S21 Nyquist Plots at temperatures (20-120 ℃) of AuNPs-1 /WO_3 and pure WO_3 films.

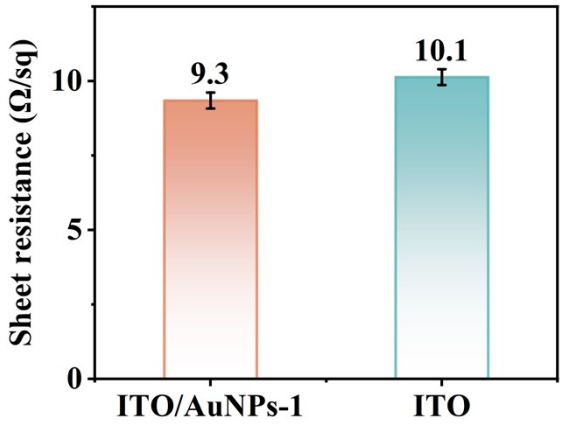

Fig. S22 Statistical diagram of sheet resistance of ITO/AuNPs-1 and ITO films.

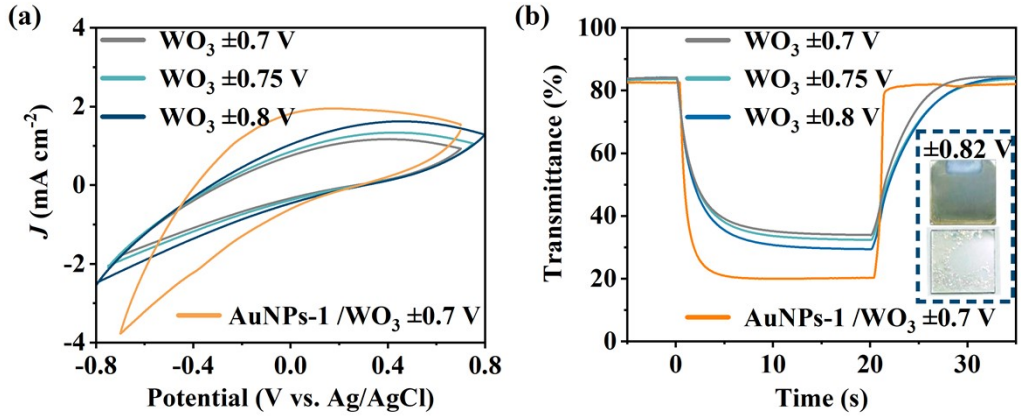

Fig. S23 CV curves of WO_3 film at different potentials and AuNPs-1 /WO_3 film at ±0.7 V. (b) In situ transmittance vs. time curves at 700 nm with different potentials of WO3 and AuNPs-1 /WO_3 films. The insets are photographs after applying ±0.82 V, the WO_3 film are damaged under this condition.

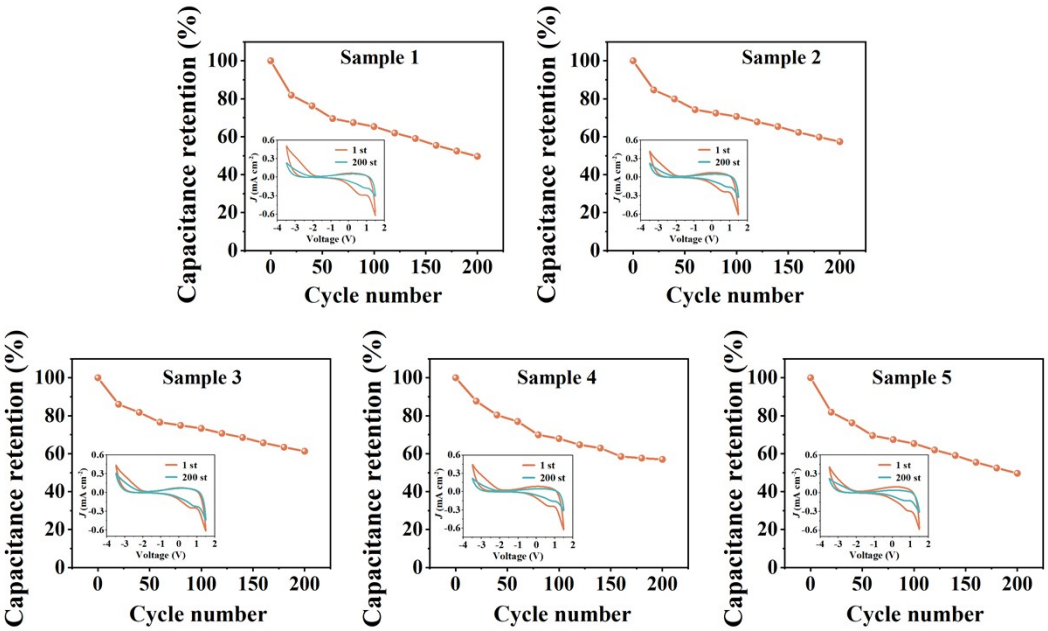

Fig. S24 Curves of capacitance retention rate of AuNPs/WO_3 versus cycle number, with the inset showing CV curves during the cycling process.

Table S1 Performance comparison of noble metal-based electrochromic films.

EC films	t_b/t_c (s)	Δ*T*@ wavelength (nm)	*CE* ($cm^2\ C^{-1}$)	Preparation Method	Flexibility	Thickness (nm)	Film size (cm)	Ref.
NiO nanocrystals	2.91/1.77	41.5 %/550	114.7	spin-coating (dry:200℃)	no	--	3×2	S1
WO_3 nanotrees	2.64/7.28	74.7 %/630	75.35	two-step solvothermal (heating:180℃)	no	465	2×2.5	S2
Wedge-like WO_3	5.0/3.4	25 %/550	35.5	dip-coating (180℃)	no	350	1×1	S3
WO_3 core/shell nanorod	15/21	67.7 %/800	101	spin coating (annealing:250℃)	no	300	1×5	S4
C-WO_3/Cu	3.2/4.5	55.35 %/600	102.3	hydrothermal (annealing:550℃)	no	600	1×1	S5
FTO/Au (20 nm)/TiO_2	6.1/8.1	40 %/700	24	co-axial electrospinning (annealing:550℃)	no	400	1×1	S6
FTO/WO_3-AuPRs (NPs: 60 nm nanorods:20×80 nm)	3.0/4.4	70 %/630	88	seed-growth and electrodeposition (annealing:350℃)	no	850	1.5×3	S7

CoS_2/WO_3	3.7/4.1	73.31 %/700	64.5	spin-coating drop-casting (annealing:60℃)	no	600	2.5×2.5	S8
WO_3-Ag (13 nm)	4.4/5.3	39.65 %/632.8	74.2	physical vapor deposition (annealing:375℃)	no	344	2× 0.9	S9
WO_3 nanofilm	12.4/10.7	69.7 %/700	72.5	hydrothermal (sealing:120℃)	no	755	1×4.8	S10
WO_3 quantum-dot	7.5/4.0	77.4 %/580	101.7	solvothermal (heating:180℃)	no	200	--	S11
WO_3	11.5/7.0	83 %/633	68.3	spin-coating (annealing:300℃)	no	346	3×3	S12
Nb-doped WO_3	15/3	54.9 %/630	61.1	sputter deposition	no	141	--	S13
WO_3@Nd-Co_3O_4	12.3/6.9	79.3 %/600	107.3	electrodeposition (annealing:450℃)	no	285	1×2.5	S14
WO_3	4.5/3.5	66.1 %/633	40.5	hydrothermal (annealing:300℃)	no	510	1.5×3	S15
ITO/AuNPs-1 /WO_3	**2.0/0.7**	**60 %/700**	**187 (BE=680)**	**E-beam Evaporation (room temperature)**	**yes**	**150**	**1.8×1.8**	**Our work**

Reference

S1. Z. Q. Xie, X. Li, Y. Zhang et al., *Mater. Today Commun*., 2019, **21**, 100635.

S2. Y. Li, W. A. McMaster, H. Wei et al., *ACS Appl. Energy Mater.*, 2018, **1**, 2552-2558.

S3. S. Adhikari, R. Swain, D. Sarkar and G. Madras, *Mol. Catal*., 2017, **432**, 76-87.

S4. X. T. Huo, Y. Li, H. Wei et al., *J. Mater. Chem. A*, 2019, **7**, 16867-16875.

S5. L. Zhao, S. S. Nie, H. X. Han et al., *Appl. Surf. Sci*., 2025, **713**, 164311.

S6. C. Eyovge, S. Kaya, M. O. Guler et al., *ACS Appl. Nano Mater.*, 2021, **4**, 8600-8610.

S7. J. W. Xu, Y. Zhang, L. Wang et al., *ACS Nano*, 2018, **12**, 6895-6903.

S8. K. Ahmad, M. A. Shinde, G. Song et al., *Ceram. Int*., 2023, **49**, 10119-10129.

S9. S. Hoseinzadeh, R. Ghasemiasl, A. Bahari et al., *J. Mater. Sci.: Mater. Electron*., 2017, **28**, 14855-14863.

S10. Y. X. Wang, I. M. Zeng, Z. H. Zhou et al., *Appl. Surf. Sci.*, 2022, **573**, 151603.

S11. D. Yang, S. Deng, Z. Jin et al., *Commun. Mater.,* 2026, **7**, 106.

S12. J. S. Fang, Y. Gong, L. K. Wang et al., *Opt. Mater.*, 2026, **174**, 117902.

S13. A. K. Mak, D. Uysal et al., *J. Alloys Compd.*, 2025, **1031**, 181040.

S14. P. J. Morankar, R. U. Amate et al., *Chem. Eng. J.*, 2025, **524**, 169630.

S15. J. Wu, L. Zhao et al., *Ceram. Int*., 2025, **51**, 35202-35213.